Sparse-Representation-Based Adaptive Interference Suppression

Yishu Shi, Feng-Xiang Ge, Ying Chen
College of Information Science and Technology
Beijing Normal University
Beijing, China
yishu.shi@mail.bnu.edu.cn

Suiling Ren
State Key Laboratory of Acoustics
Institute of Acoustics, Chinese Academy of Sciences
Beijing, China

***Abstract*—Passive sources localization in the presence of strong interferences is generally a difficult problem. A sparse-representation-based adaptive interference suppression (SRAIS) method is proposed in this paper for interference suppression and bearing estimation, which can reduce the power loss of the TOI signal and have more accurate direction-of-arrival (DOA) estimation, especially when the input powers of the TOI signal and the interferences are at the almost same level. Simulation and experimental results are also given.**

***Keywords*—adaptive interference suppression; sparse representation; direction of arrival estimation**

I. INTRODUCTION

Passive sonar localization in shallow water in the presence of interferences is generally a very difficult task. The sidelobes associated with the interferences could severely mask the location of sources. Therefore, effective adaptive interference suppression becomes essential.

Adaptive interference suppression can increase the signal-to-interference ratio (SIR) processing gain and also have adaptivity to fluctuations in interference and noise statistics [1]–[3]. The constrained minimum variance distortionless response (MVDR) criterion aims to cancel or suppress the interference output and preserve the response at the TOI bearing. However, *a priori* knowledge of the accurate bearings of both the interference and TOI is required. Subspace-based analysis [4]–[10] has also been proposed for the problem. For example, the principal component inverse (PCI) in [4] and [5] and the dominant mode rejection (DMR) in [6]–[9] both operate in a reduced dimension space consisting of the eigenvectors associated with the large eigenvalues of the cross-spectral density matrix (CSDM). These large eigenvectors are assumed to be associated with the space spanned by the TOI signals and the interferences. However, varying propagation conditions may mix the subspace composition. Therefore, the separation of interference and TOI is always a hard task. For instance, the adaptive eigencomponent association (ECA) method in [11], related to the technique from [10], adaptively identifies the components dominated by interferences according to a defined power ratio, assuming *a priori* knowledge regarding the accurate bearing of the TOI. Unfortunately, the threshold value of that power ratio relies on many practical factors, such as signal-to-noise ratio (SNR), SIR, the coherence between the interferences and the TOI signal, etc. The eigenanalysis-based adaptive interference suppression (EAAIS) method in [12] can adaptively remove the eigenvector dominated by interferences without the accurate bearing of the TOI and the number of the sources (e.g., the interferences and TOI) by a fixed contribution ratio. The reconstructed CSDM with conventional beamforming (CBF) [12] can be taken for estimating the TOI bearing. However, when input powers of the target of interest (TOI) signal and the interferences are at the almost same power level or closely spaced, the EAAIS method will be subjected to power loss and identification problem.

In this paper, a sparse-representation-based adaptive interference suppression (SRAIS) method is proposed. The CSDM is reconstructed with the atoms dominated by the TOI. The simulation and experimental results show the SRAIS method can reduce the power loss of the TOI signal and have more accurate direction-of-arrival (DOA) estimation, especially when the TOI signal and the interferences are at the almost same power level or closely spaced.

II. SPARSE -REPRESENTATION-BASED ADAPTIVE INTERFERENCE SUPPRESSION

A. CSDM Restruction Based on Sparse-Representation

For a horizontal line array (HLA) consisting of *M* elements equally spaced with interval Δ, the pressure field measured by the *m*th element at the *k*th snapshot and the frequency ω_l can be expressed as

$$x_m(\omega_l,k)=\sum_{j=0}^{J} s_j(\omega_l)\, H_m\left(\omega_l, r_j(k)\right)+n_m(\omega_l,k),\quad m=1,2,\dots,M \quad (1)$$

where $n_m(\omega_l,k)$ denotes the additive white Gaussian noise (AWGN); $s_0(\omega_l)$ and $s_j(\omega_l)$, for $j=1,2,\dots,J$, denote the spectra of the TOI signal and the *j*th interference, respectively; $H_m\left(\omega_l, r_j(k)\right), j=1,2,\dots,J$, denotes the transfer function between the *m*th element and the *j*th source (e.g., the interferences and TOI). The transfer function can also be expressed in terms of the normal modes [13] as

$$H_m\left(\omega_l, r_j(k)\right)=\sum_n A_n(\omega_l, r_j(k)+r_m, z, z_j)\, e^{j[k_n(\omega_l)(r_j(k)+r_m)+\frac{\pi}{4}]} \quad (2)$$

where $A_n(\omega_l, r_j(k)+r_m, z, z_j)$ and $k_n(\omega_l)$ denote the *n*th mode amplitude and horizontal wave number, respectively,

$r_j(k)$ is the distance from the jth source to the first element of the array, $r_m = (m-1)\Delta\cos\phi_j$ and $r_j(k) + r_m$ is the distance from the jth source to the mth element, and ϕ_j and z_j are the bearing and depth of the jth source, respectively. The bearing is relative to endfire. All elements of the HLA are at the same depth. In this paper, we assume that there is only one TOI. The derivation for multiple TOIs is relatively straightforward and thus omitted. The TOI bearing is $\phi_{\mathrm{TOI}} = \phi_0$.

The CSDM of observation formed with K snapshots in the tth frame can be expressed as

$$\boldsymbol{R}_x(\omega_l, t) = \frac{1}{K}\sum_{k=1}^{K} \boldsymbol{x}(\omega_l, k)\boldsymbol{x}^{\mathrm{H}}(\omega_l, k) \tag{3}$$

where $\boldsymbol{x}(\omega_l, k) = [x_1(\omega_l, k) \dots x_m(\omega_l, k) \dots x_M(\omega_l, k)]^{\mathrm{T}}$ and superscripts T and H denote the transpose and conjugate transpose of a vector or a matrix, respectively.

The sparse representation of $\boldsymbol{R}_x(\omega_l, t)$ can be computed with the number of the sources by the l_1-ACMSR algorithm as in [14]. The dictionary $\mathbf{A}(\omega_l, \boldsymbol{\phi})$ is based on the array manifold, whose pth column is the pth signal array steering vector $\boldsymbol{a}(\omega_l, \phi_p) = [1, \mathrm{e}^{j\omega_l \Delta\cos\phi_p / c_0}, \dots, \mathrm{e}^{j\omega_l (M-1)\Delta\cos\phi_p / c_0}]^{\mathrm{T}}$,where ω_l is the frequency, and c_0 is the sound speed.

Then the sparse representation of one row in $\boldsymbol{R}_x(\omega_l, t)$ can be obtained as in (4), theoretically,

$$\begin{aligned} &\min \|\boldsymbol{\lambda}(\omega_l, t)\|_1 \\ &\text{subject to } \mathbf{A}(\omega_l, \boldsymbol{\phi})\boldsymbol{\lambda}(\omega_l, t) = \boldsymbol{r}_x(\omega_l, t) \end{aligned} \tag{4}$$

where $\|\boldsymbol{\lambda}\|_1$ denotes l_1-norm. Then we have

$$\boldsymbol{R}_x(\omega_l, t) = \sum_{m=1}^{M} \lambda_m(\omega_l, t)\boldsymbol{a}(\omega_l, \phi_m, t)\boldsymbol{a}^{\mathrm{H}}(\omega_l, \phi_m, t) \tag{5}$$

where $\lambda_m(\omega_l, t)$ and $\boldsymbol{a}(\omega_l, \phi_m, t)$ denote the mth coefficient and atom of $\boldsymbol{R}_x(\omega_l, t)$, respectively. Thus, the CBF of the atom can be expressed as

$$BA_m(\omega_l, \phi, t) = \boldsymbol{b}^{\mathrm{H}}(\omega_l, \phi)\boldsymbol{a}(\omega_l, \phi_m, t)\boldsymbol{a}^{\mathrm{H}}(\omega_l, \phi_m, t)\boldsymbol{b}(\omega_l, \phi) \tag{6}$$

where $\boldsymbol{b}(\omega_l, \phi) = \boldsymbol{a}(\omega_l, \phi)/M$, M is the number of the array sensors, $BA_m(\omega_l, \phi, t)$ in (6) can be interpreted as the contribution of the source at the bearing ϕ to the atom associated with $\boldsymbol{a}(\omega_l, \phi_m, t)$. Therefore, if we can identify the atoms dominated by the TOI or the interferences, the components of the CSDM can be better separated for interference suppression.

A contribution ratio (CR) with those atoms is then defined as follows

$$\mathrm{CR}_m = \frac{\max_{\phi \in \Phi_{\mathrm{T}}} BA_m(\omega_l, \phi, t)}{\max_{\phi \in [0°, 180°]} BA_m(\omega_l, \phi, t)}, \quad m = 1, 2, \dots, M. \tag{7}$$

It is expected that the atoms associated with the TOI are adaptively identified and reserved for interference suppression and SNR improvement. In this paper, we assume the TOI bearing is in a known bearing sector Φ_{T}, i.e., $\phi_{\mathrm{TOI}} \in \Phi_{\mathrm{T}}$ and $\phi_{\mathrm{I}_j} \notin \Phi_{\mathrm{T}}$, for $j = 1, 2, \dots, J$, where ϕ_{I_j} denotes the bearing of the jth interference. Several properties of the CR in (7) are given below.

1) If the mth atom $\boldsymbol{a}(\omega_l, \phi_m, t)$ is dominated by the TOI, the bearing corresponding to the peak response of $BA_m(\omega_l, \phi, t)$ should be in Φ_{T} and, therefore, $\mathrm{CR_m} = 1$. Let $\boldsymbol{a}(\omega_l, \phi_m, t) \in \widetilde{\boldsymbol{A}}_T(\omega_l, t)$, where $\widetilde{\boldsymbol{A}}_T(\omega_l, t)$ denotes the set of atoms not dominated by the interferences.

2) If the dominant contribution to the mth atom $\boldsymbol{a}(\omega_l, \phi_m, t)$ is from the interferences that are located out of Φ_{T}, we must have $\mathrm{CR_m} < 1$. Let $\boldsymbol{a}(\omega_l, \phi_m, t) \in \widetilde{\boldsymbol{A}}_I(\omega_l, t)$, where $\widetilde{\boldsymbol{A}}_I(\omega_l, t)$ denotes the set of atoms not dominated by the TOI.

3) If the dominant contribution to the mth atom $\boldsymbol{a}(\omega_l, \phi_m, t)$ is from the noise, it can be separated into $\widetilde{\boldsymbol{A}}_T(\omega_l, t)$ and $\widetilde{\boldsymbol{A}}_I(\omega_l, t)$, respectively, to increase the output SNR.

Then, we have

$$\begin{aligned} \mathrm{CR}_m < 1 &\rightarrow \boldsymbol{a}(\omega_l, \phi_m, t) \in \widetilde{\boldsymbol{A}}_I(\omega_l, t) \\ \mathrm{CR}_m = 1 &\rightarrow \boldsymbol{a}(\omega_l, \phi_m, t) \in \widetilde{\boldsymbol{A}}_T(\omega_l, t) \end{aligned} \tag{8}$$

The Interferences can be removed from CSDM as follows

$$\overline{\boldsymbol{R}_x}(\omega_l, t) = \boldsymbol{P}_{\perp}(\omega_l, t)\boldsymbol{R}_x(\omega_l, t)\boldsymbol{P}^{\mathrm{H}}{}_{\perp}(\omega_l, t) \tag{9}$$

where $\overline{\boldsymbol{R}_x}(\omega_l, t)$ is the reconstructed CSDM, $\boldsymbol{P}_{\perp}(\omega_l, t) = \widetilde{\boldsymbol{A}}_T(\omega_l, t)\widetilde{\boldsymbol{A}}_T{}^{\mathrm{H}}(\omega_l, t)$ is the projection matrix. The sparse representation finds a set of mutually basis functions that capture the directions of maximum coefficients in the data. Whether the sources are incoherent and orthogonal to each other or not, each atom will only correspond to one direction, which means one source, and will not leak its energy into other atoms.

B. Bearing Estimation Based on SRAIS-CBF

The reconstructed CSDM with CBF is taken for better TOI bearing estimation.

$$\bar{B}(\phi, t) = \frac{1}{L}\sum_{l=1}^{L} \boldsymbol{b}^{\mathrm{H}}(\omega_l, \phi)\overline{\boldsymbol{R}_x}(\omega_l, t)\boldsymbol{b}(\omega_l, \phi) \tag{10}$$

where L is the number of frequency bins in the frequency band of interest. The maximum of $\bar{B}(\phi, t)$ correspond to the estimated bearings of sources by SRAIS–CBF (so as CBF, and EAAIS-CBF [12]) in the tth frame, respectively, that is

$$\hat{\phi}_{\mathrm{SR}}(t) = \arg\max_{\phi} \bar{B}(\phi, t) \tag{11}$$

Consequently, $\hat{\phi}_{\mathrm{SR}}(t) = \hat{\phi}_{\mathrm{TOI\_SR}}(t)$ correspond to the estimated bearings of the TOI by SRAIS–CBF (so as CBF and EAAIS-CBF), respectively.

III. Performance of SRAIS and Discussion

A. Simulation and Discussion

A comparison of CBF, EAAIS–CBF, and SRAIS–CBF for bearing estimation is shown in Fig. 1(a) and (b). In the simulations, we consider an HLA with 48 elements equally spaced at an interval of 2.5m. The bearing is relative to endfire. The sound speed is $c_0 = 1500\mathrm{m/s}$, the frequency of interest is $\omega = [200\ \mathrm{Hz}, 300\ \mathrm{Hz}]$, the number of frequency bins is set to $L = 14$, and the number of snapshots is $K = 148$. Two interferences and one weak TOI are assumed in Fig. 1.

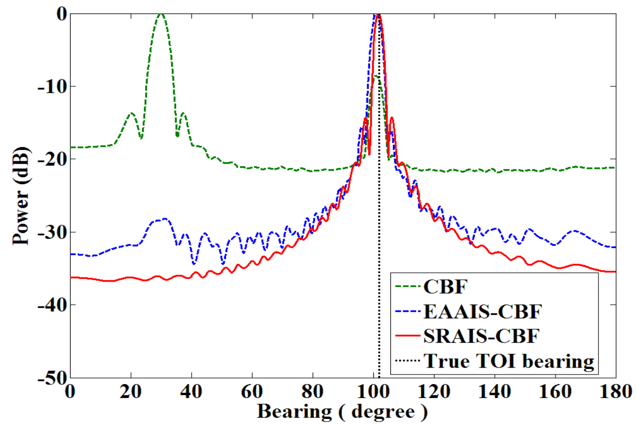

(a)

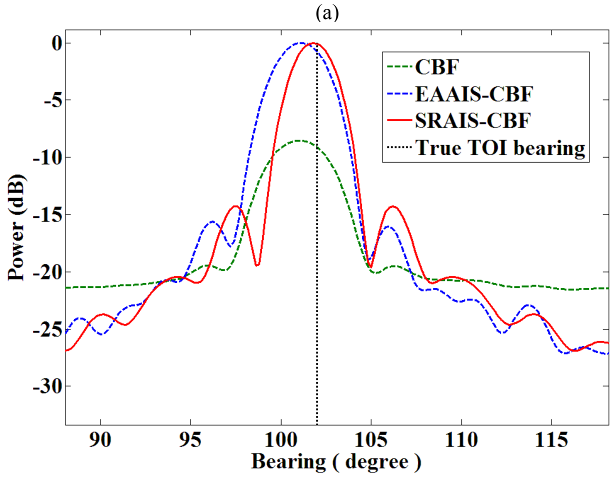

(b)

Fig. 1. Normalized output powers of CBF, EAAIS–CBF, and SRAIS–CBF

In Fig. 1, the TOI signal is at $\phi_{\mathrm{TOI}} = 102°$ with $\mathrm{SNR} = -5\mathrm{dB}$. One interference is at 30° with $\mathrm{SIR} = 0\mathrm{dB}$ and the other is at 99° with $\mathrm{SIR} = -10\mathrm{dB}$. The bearing sector for the TOI is set to [100°, 104°].

In Fig. 1(a), it is shown that SRAIS–CBF has the more accurate TOI bearing estimate, mainly because of the reduced contribution of interferences in the reconstructed $\overline{\boldsymbol{R}_{x}}(\omega_l, t)$. In comparison, CBF-based and EAAIS-CBF-based TOI bearing estimate is completely masked by the first sidelobe of the second interference at 99°. In addition, since the atoms dominated by the noise may also be excluded in the SRAIS–CBF method, which make SRAIS–CBF have higher SNR processing gain. The beamformer outputs in a smaller bearing sector are shown in Fig. 1(b) for better performance comparison of the different DOA estimation methods.

B. Power Loss Discussion

In PCI, ECA and EAAIS, the eigendecomposition of the CSDM essentially finds the directions of maximal variance based on l_2-norm [15]. Each principal eigenvector corresponds to one source if the sources are incoherent and perfectly orthogonal to each other. In practical applications, however, this is not necessarily true. The interferences may not be completely incoherent with the TOI signal, also due to the array aperture, sampling frequency, common perturbations, etc. Then the TOI signal and the interferences may be mixed in one or more principal eigenvectors. Thus the interferences may not be suppressed completely by the EAAIS–CBF method and the TOI signal may be subject to power loss. In this paper, we reconstruct the CSDM with most associated atoms, where the optimization is based on both l_1-norm and l_2-norm.

Fig. 2(a) shows the power loss of TOI signal versus SIR. Two sources are considered in this simulation. The TOI is at $\phi_{\mathrm{TOI}} = 30°$ and $\mathrm{SNR} = -5\mathrm{dB}$. The interference is at $\phi_{\mathrm{I}} = 35°$ and the SIR is from −35 to 10dB. The power loss can be calculated by subtracting the output power (dB) of SRAIS-CBF at the TOI bearing from the input power (dB) of the TOI signal plus the array processing gain (dB) before normalization. As shown in Fig. 2(a), the maximum power loss of EAAIS-CBF appears when the SIR is about 0 dB, but not shown in SRAIS-CBF. The negative power loss also appears at the low and high SIR regions in Fig. 3(a). Since the white Gaussian noise in the measurement may be assumed isotropic, hence is involved in each principal eigenvector, negative power loss occurs to EAAIS-CBF when the TOI signal does not leak energy to other eigenvectors. Since SRAIS-CBF can reduce the white Gaussian noise in associated atoms. Fig. 2(b) shows the SRAIS method also have more accurate direction-of-arrival estimates than EAAIS. $\mathrm{SIR} = 0\mathrm{dB}$ in Fig. 2(b).

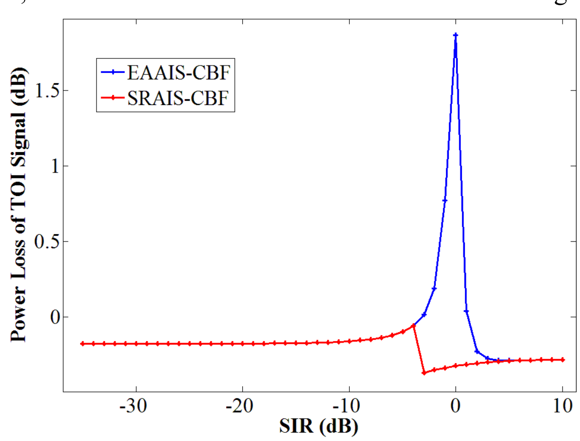

(a)

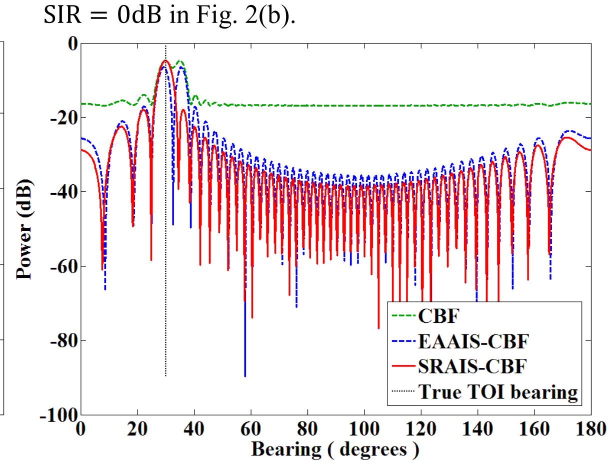

(b)

Fig. 2. Power loss of TOI signal Versus SIR. $\phi_{\mathrm{TOI}} = 30°, \phi_{\mathrm{I}} = 35°, \mathrm{SNR} = -5$ dB.

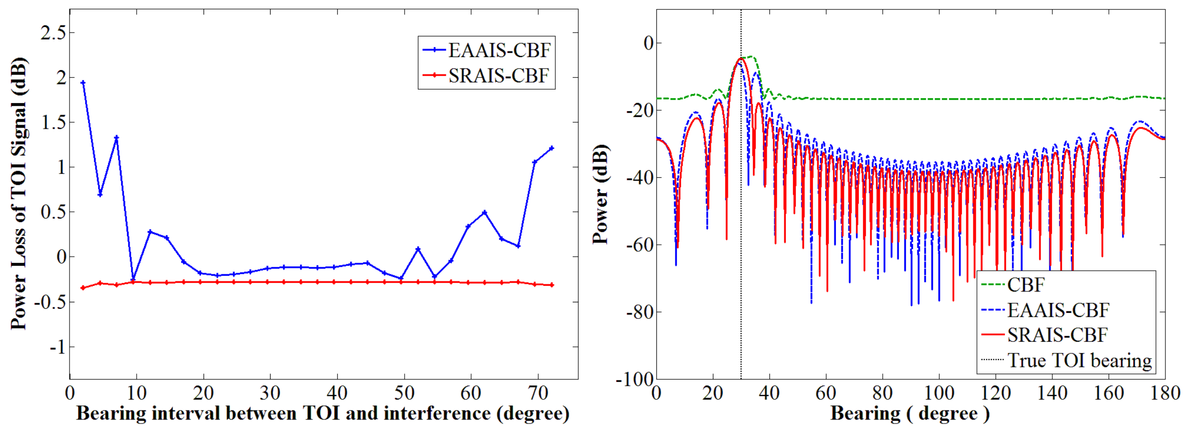

(a) (b)

Fig. 3. Power loss of TOI signal versus the bearing interval between the TOI and interference. $\phi_{\mathrm{TOI}} = 30°$, $\Phi_{\mathrm{I}} = [34°, 178°]$, $\mathrm{SNR} = -5$ dB, $\mathrm{SIR} = -1$ dB.

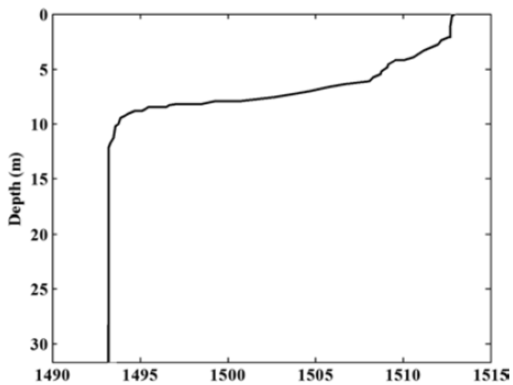

Fig. 4. Sound-speed profile

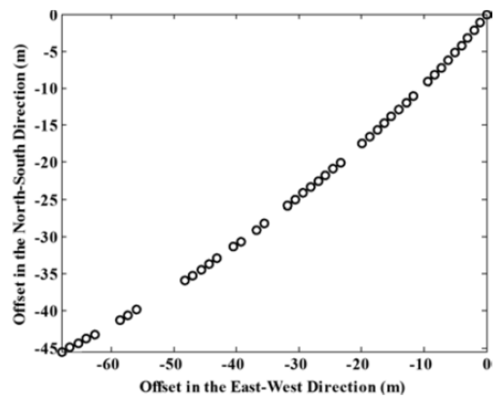

Fig. 5. Deployment of the horizontal array.

Fig. 3(a) shows the power loss of TOI signal versus the bearing interval between the TOI and the interference at $\mathrm{SIR} = -1\mathrm{dB}$. The TOI is at $\phi_{\mathrm{TOI}} = 30°$ and the bearing of the interference varies from 34° to 178°, and $\mathrm{SNR} = -5\mathrm{dB}$. It is shown in Fig. 3 that the SRAIS method not only reduce the power loss of the TOI signal, but also have more accurate direction-of-arrival estimates.

C. Experimental Results

The input data were collected from an acoustic experiment in the Yellow Sea conducted in June 2005. The sound-speed profile (SSP) measured in the experiment is shown in Fig. 4. A horizontal array with 43 elements spaced at about 1.5-m interval was deployed on the seabed, as illustrated in Fig. 5. The moving ships were considered as the acoustic sources.

The bearing-time distributions estimated using the CBF, EAAIS-CBF, and SRAIS-CBF methods are illustrated in Fig. 6(a)-(c), respectively. The bearing is relative to the true north. The bearing track of the TOI is marked in Fig. 6(a), and the Global Positioning System (GPS)-recorded bearing track is shown by the dashed line in Fig. 6(a)-(c). Since the acoustic array deployed in the experiment was approximately linear, as shown in Fig. 5, the bearing tracks of the TOI and the interferences are mirrored at about 57° and 237°. For the EAAIS–CBF, and SRAIS-CBF methods and the initial bearing sector in the first frame, is set to [108°, 112°] as *a priori* knowledge. The bearing sector in the *t*th frame $\Phi_{\mathrm{T}}(t)$ can be adaptively adjusted as follows: $\Phi_{\mathrm{T}}(t) = [\phi_{\mathrm{TOI}}(t-1) - \Delta\phi, \phi_{\mathrm{TOI}}(t-1) + \Delta\phi]$, while $\Delta\phi = 2°$and $\phi_{\mathrm{TOI}}(t-1)$ is the TOI bearing estimate in the last frame [i.e., the $(t-1)$th frame] by those method. Then, the procedure described by (6)–(11) is used to track the TOI bearing. Fig. 6 (c) shows a much clearer bearing-time distribution and interference suppression as compared to that in Fig. 6(a)-(b). This suggests that the interferences and the noise effects have been effectively suppressed and the TOI is accurately tracked by the SRAIS–CBF method.

The experimental results for bearing estimation using the CBF, EAAIS–CBF, and SRAIS–CBF methods are illustrated in Fig. 7(a), (b) and (c), for three different frames, respectively. According to the TOI bearing in the last frame [$\phi_{\mathrm{T}}(t = 3.9\ \mathrm{min}) = 123°, \phi_{\mathrm{T}}(t = 14.9\ \mathrm{min}) = 128°, \phi_{\mathrm{T}}(t = 30.3\ \mathrm{min}) = 129°$], the TOI bearing sectors for SRAIS and EAAIS are $\Phi_{\mathrm{T}}(t = 4\ \mathrm{min}) = [121°, 125°]$, $\Phi_{\mathrm{T}}(t = 15\ \mathrm{min}) = [126°, 130°]$ and $\Phi_{\mathrm{T}}(t = 30.4\ \mathrm{min}) = [127°, 131°]$. All the outputs have been normalized by their peak responses to better illustrate the output SNR and SIR. It is showed that the SRAIS–CBF method achieves higher SNR and SIR gains compared to CBF and EAAIS–CBF. Fig. 7(d), (e) and (f) illustrate the part of outputs of Fig. 7(a), (b) and (c) for clearer comparison, and show that SRAIS-CBF achieved more accurate DOA estimation than EAAIS-CBF and CBF.

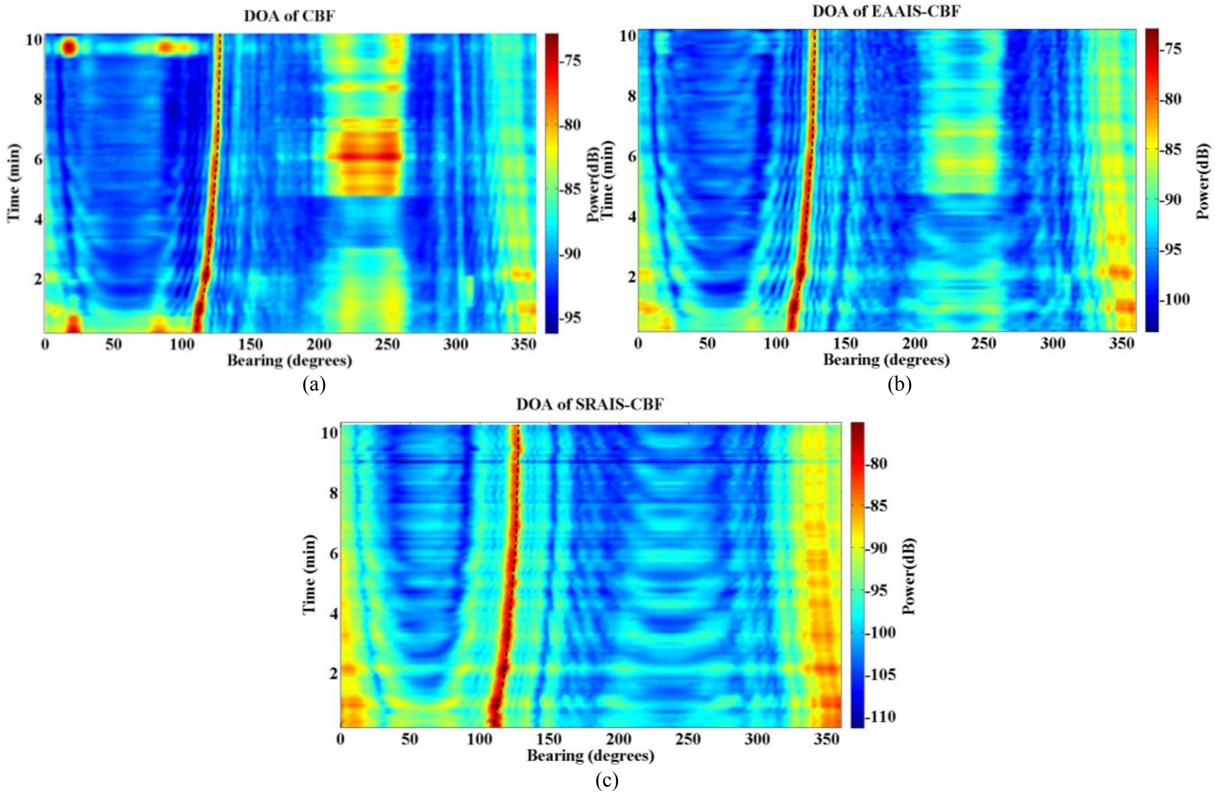

Fig. 6. Bearing-time distribution estimated by (a) CBF, (b) EAAIS-CBF, and (c) SRAIS–CBF. $M = 43, \omega \in [200\ \text{Hz}, 250\ \text{Hz}], L = 53, K = 6, c_0 = 1493\ \text{m/s}$.

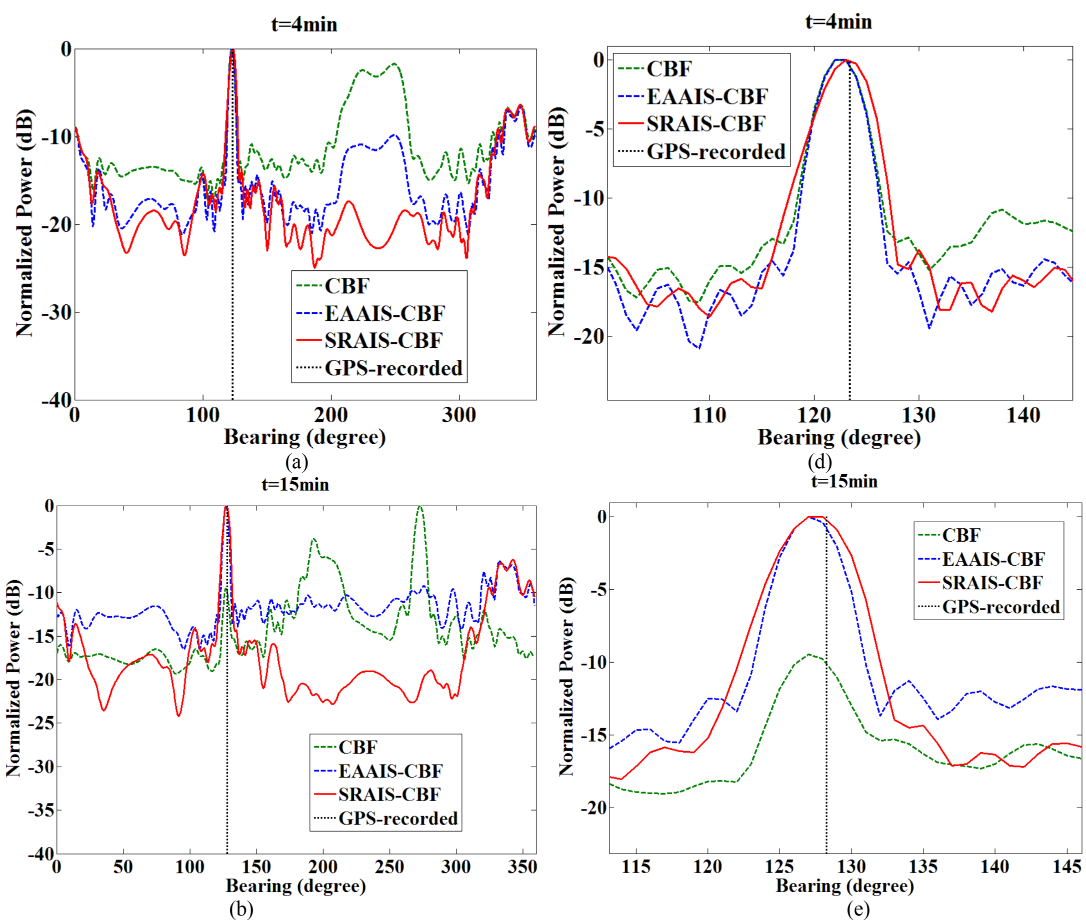

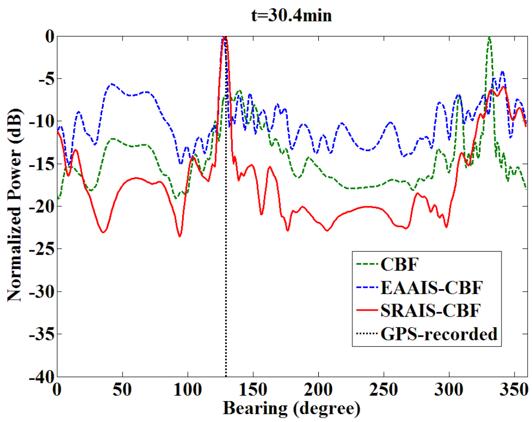

(c)

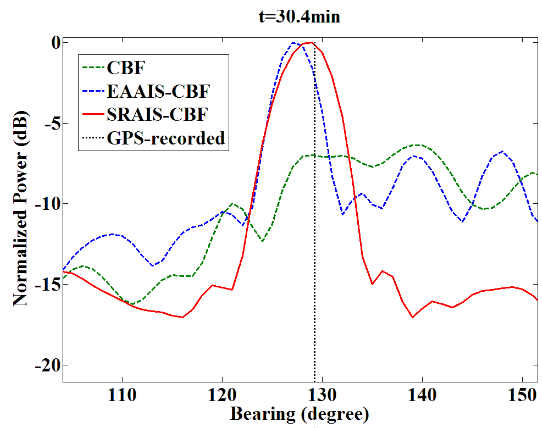

(f)

Fig. 7. Output powers of CBF, EAAIS–CBF, and SRAIS–CBF for three different frames (a) at 4 min($\Phi_{\mathrm{T}}(t = 4\text{min}) = [121°, 125°]$), (b) at 28min($\Phi_{\mathrm{T}}(t = 15 \text{ min}) = [126°, 130°]$)and (c) at 30.4 min($\Phi_{\mathrm{T}}(t = 30.4 \text{ min}) = [127°, 131°]$). (d) Part of (a) in a smaller bearing sector. (e) Part of (b) in a smaller bearing sector. (f) Part of (c) in a smaller bearing sector. $M = 43, \omega \in [200 \text{ Hz}, 250 \text{ Hz}], L = 53, K = 6, c_0 = 1493 \text{ m/s}$.

IV. CONCLUSION

In this paper, the SRAIS method has been presented for the adaptive interference suppression and passive acoustic source bearing estimation. Based on the sparse representation and a CR, we can adaptively identify the atoms associated with the TOI signal. The identified atoms were then used to reconstruct CSDM for interference suppression, and thus the bearing estimation is improved, especially for the weak TOI signals. The simulation and experimental results demonstrated the significant performance improvement in both interference suppression and bearing estimation.

REFERENCES

[1] H. Krim and M. Viberg, “Two decades of array signal processing research,” IEEE Signal Process. Mag., vol. 13, no. 4, pp. 67–94, Jul. 1996.

[2] R. J. Vaccaro, “The past, present and future of underwater acoustic signal processing,” IEEE Signal Process. Mag., vol. 15, no. 4, pp. 21–51, Jul. 1998.

[3] R. J. Mailloux, “Covariance matrix augmentation to produce adaptive array pattern troughs,” Electron. Lett., vol. 31, no. 10, pp. 771–772, 1995.

[4] I. P. Kirstens and D.W. Tufts, “On the probability density of signal-tonoise ratio in an improved adaptive detector,” in Proc. IEEE Int. Conf. Acoust. Speech Signal Process., 1985, vol. 10, pp. 572–575.

[5] I. P. Kirsteins and D. W. Tufts, “Adaptive detection using low rank approximation to a data matrix,” IEEE Trans. Aerosp. Electron. Syst., vol. 30, no. 1, pp. 55–67, Jan. 1994.

[6] N. L. Owsley, “Enhanced minimum variance beamforming,” in Underwater Acoustic Data Processing, ser. NATOAS1, Y.Chan, Ed. Norwell, MA, USA: Kluwer, 1989.

[7] D. A. Abraham and N. L. Owsley, “Beamforming with dominant mode rejection,” in Proc. IEEE OCEANS Conf., 1990, pp. 470–475.

[8] H. COX and R. Pitre, “Robust DMR and multi-rate adaptive beamforming,” in Proc. 31st Asilomar Conf. Signals Syst. Comput., 1998, vol. 1, pp. 920–924.

[9] H. Cox, “Multi-rate adaptive beamforming (MRABF),” in Proc. Sensor Array Multichannel Signal Process. Workshop, 2000, pp. 306–309.

[10] S. M. Kogon, “Robust adaptive beamforming for passive sonar using eigenvector/beam association and excision,” in Proc. Sensor Array Multichannel Signal Process. Workshop, 2002, pp. 33–37.

[11] B. F. Harrison, “The eigencomponent association method for adaptive interference suppression,” J. Acoust. Soc. Amer., vol. 115, no. 5, pp. 2122–2128, 2004.

[12] S. Ren, F.-X. Ge, X. Guo, and L. Guo, “Eigenanalysis-Based Adaptive Interference Suppression and Its Application in Acoustic Source Range Estimation,” accepted for publication by IEEE Journal of Oceanic Engineering, 2015.

[13] L. Brekhovskikh and Y. Lysanov, Fundamentals of Ocean Acoustics, 3rd ed. New York, NY, USA: AIP, 2003.

[14] Z. Q. He, Q. H. Liu, L. N. Jin and S. Ouyang, “Low complexity method for DOA estimation using array covariance matrix sparse representation,” Electronics Letters, vol. 49, no. 3, 2013.

[15] X. F. He,D. Cai, and W.Min, “Statistical and computational analysis of locality preserving projection,” in Proc. 22nd Int. Conf. Mach. Learn., 2005, pp. 281–288